BUTTERWORTH HEINEMANN

Polymer Vol. 36 No. 2, pp. 299–308, 1995

0032-3861/95/$10.00+0.00

Rate dependent and network phenomena in the multiaxial drawing of poly(vinyl chloride)

J. Sweeney and I. M. Ward*
IRC in Polymer Science and Technology, University of Leeds, Leeds LS2 9JT, UK
(Received 7 December 1993; revised 4 July 1994)

Stress–strain data have been obtained for poly(vinyl chloride) from drawing experiments in three stretching modes: uniaxial, planar and equibiaxial extension. The experiments were conducted isothermally at 84°C, which is in the glass transition region, and at 90°C, above T_g. The stress–strain behaviour is qualitatively different at the two temperatures. At the lower temperature, there is an initial stiff response followed by a decrease in slope suggestive of yielding, whereas this effect is absent at 90°C. There is strain rate dependence at both temperatures, with stress simply related to the logarithm of the shear rate. To model the behaviour above the glass transition, strain rate dependence is included in a network model; the alternative of a time independent network acting in parallel with a yielding process is found to be inadequate. At the lower temperature, however, there is a need for such a process acting in parallel with the time dependent network in order to predict adequately the initial shapes of the stress–strain curves. The resulting constitutive equations provide very good representations at both temperatures.

(Keywords: poly(vinyl chloride); orientation; multiaxial drawing)

INTRODUCTION

Macroscopic studies of the deformation of polymers can give insight into events at a molecular level. They are also of interest from an engineering point of view, since knowledge of the constitutive stress–strain equations is the key to the successful modelling of many polymer-forming processes. In this paper we address the problem of a polymer of low crystallinity, poly(vinyl chloride) (PVC), when oriented mechanically into various states of large deformation. Its constitutive behaviour when being stretched at high temperatures is analysed using the concept of a sliplink network to which some rate dependent behaviour has been added.

Our experiments were at temperatures within the glass transition or above it. The yield behaviour of PVC at these temperatures has been examined by Bauwens *et al.*[1]. Their study was confined to uniaxial tensile behaviour and showed that the rate dependence of yield stress could be modelled in terms of a modified Eyring theory; they did not explore network effects. The general importance of molecular networks in the deformation of polymers is a key concept in the understanding of rubber elasticity, and has been established more generally as a result of the study of molecular orientation, for example by spectroscopic techniques[2]. In a review by Ward[3], polymer deformation is discussed as a combination of both network effects and rate dependent processes. This concept has been developed in detail by Boyce *et al.*[4] for glassy polymers below the glass transition.

We have deformed sheets of unplasticized PVC into three distinct states of finite strain using a high temperature biaxial drawing machine. This has generated stress–strain curves in uniaxial, planar (constant width) and equibiaxial extension over a range of rates and at temperatures both above the glass transition and in the glass transition region. In a previous paper[5] we observed that the behaviour at the lower temperature was more rate dependent than at the higher temperature, so that in the latter case a phenomenological rubber elastic model could be used to relate stress–strain behaviour in different stretching modes at comparable rates. Here, we examine the rate dependence in both temperature regimes. Above the glass transition, the behaviour is represented very successfully using a network model in which one of the parameters is assigned a simple rate dependence. In the glass transition range, the behaviour is qualitatively different, but can be viewed as a similar network in combination with a viscosity term depending only on the deformation rate.

EXPERIMENTAL AND THEORY

The experiments were performed using a biaxial drawing machine designed and manufactured in-house. Two perpendicular stretching axes were programmed to move independently at rates which varied with time in a very general way by means of a high level real-time programming language. The drawing took place isothermally within an oven which had a viewing window. Four load cells situated outside the oven measured the total force acting on each specimen side. Initially square

* To whom correspondence should be addressed

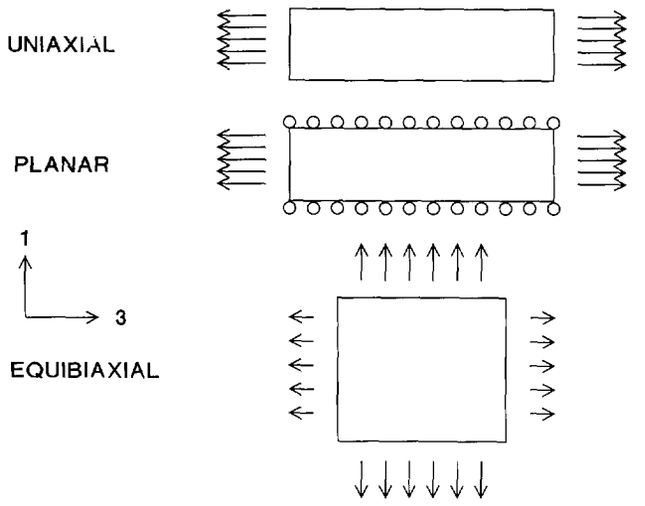

Figure 1 The three stretching modes

sheet specimens were drawn in one of the stretching modes shown in *Figure 1*: uniaxial, planar (constant width) or equibiaxial extension. A side of the specimen could be held by five grips which could slide on rollers in the direction normal to the stretch direction. In the uniaxial case, only two opposite specimen edges needed to be gripped, and then the grips moved freely inwards to produce a substantially uniform drawn specimen; however, it was possible to grip the other two edges and program the lateral axis to move inwards at a rate appropriate for uniaxial drawing. We used this procedure in some cases to ensure that the gripping arrangement, and therefore the drawing temperature, in the uniaxial case was strictly comparable with that in the other two cases.

Each specimen consisted of two 190×190 mm sheets of 300 μm film. The use of two sheets enabled thermocouples to be placed between them to give a reliable reading of the specimen temperature; the two temperatures used were 84 and 90°C. The film was Staufen type 48.4, kindly supplied by Bryan Clark at ICI Films, Welwyn Garden City. The PVC was characterized by approximate molecular weights $\bar{M}_w = 85\,000$ and $\bar{M}_n = 40\,000$, and the film contained no plasticizer but around 15% additives. The same material was used by Ward and coworkers[5,6]. In recent work[6], the glass transition temperature was measured by differential scanning calorimetry on specimens with varying levels of orientation, and the resulting range was 77–85°C.

Since the rate of straining was one of the important variables of this investigation, it was necessary to know an effective measure of it which could enable experiments in the different stretching modes to be carried out consistently. We assumed that the octahedral shear strain rate was such a measure. In the following treatment, we relate this measure to the deformation histories of the three types of experiment. Suppose the strain rate in the principal directions is $\dot{e}_{ii}$ for $i = 1$, 2 and 3. Then the octahedral shear strain rate depends on the direction of the octahedral plane, which in turn is defined by the principal stresses. Working in the 1–3 plane as in *Figure 1* with $\sigma_{22} = 0$, the octahedral shear strain rate $\dot{e}'_{13}$ is obtained by transforming the strain rate tensor onto the axis set defined by the octahedral stresses. It is given by

$$\dot{e}'_{13} = \frac{1}{9\tau_{oct}}[(2\sigma_{11} - \sigma_{33})\dot{e}_{11} - (\sigma_{11} + \sigma_{33})\dot{e}_{22} + (2\sigma_{33} - \sigma_{11})\dot{e}_{33}] \quad (1)$$

where the octahedral shear stress is in this case defined by

$$\tau_{oct} = \tfrac{1}{3}\sqrt{2(\sigma_{11}^2 + \sigma_{33}^2 - \sigma_{11}\sigma_{33})}$$

The octahedral shear stress is simply related to the von Mises or equivalent stress. In order to represent equation (1) in terms of experimental variables, we need to define the rate of strain. The classical strain rate measure of incompressible plasticity is given by $\dot{e}_{ii} = \dot{\lambda}_i/\lambda_i$ ($i = 1$ and 3). The use of this definition in equation (1) gives for uniaxial stretching in the 3 direction

$$\dot{e}'_{13} = \frac{1}{\sqrt{2}}\frac{\dot{\lambda}_3}{\lambda_3} \quad (2)$$

Similarly, for equibiaxial stretching in the 1–3 plane we obtain

$$\dot{e}'_{13} = \sqrt{2}\frac{\dot{\lambda}_3}{\lambda_3} \quad (3)$$

For the planar extension or constant width case there is less symmetry and the result involves the ratio of the principal stresses. Defining this ratio a by $\sigma_{11} = a\sigma_{33}$, the result for stretching along the 3 axis with $\lambda_1 = 1$ is given by

$$\dot{e}'_{13} = \frac{1}{\sqrt{2(a^2 - a + 1)}}\frac{\dot{\lambda}_3}{\lambda_3} \quad (4)$$

However, we have chosen to adopt the strain rate measure $\dot{e}_{ii} = \dot{\lambda}_i$ ($i = 1$ and 3). This results in definitions of the shear strain rate given by equations (5)–(7) below. For the uniaxial case

$$\dot{e}'_{13} = \frac{\sqrt{2}\dot{\lambda}_3}{3}\left(1 + \frac{1}{2}\lambda_3^{-3/2}\right) = \frac{\sqrt{2}}{3}\frac{d}{dt}(\lambda_3 - \lambda_3^{-1/2}) \quad (5)$$

For equibiaxial stretching we have

$$\dot{e}'_{13} = \frac{\sqrt{2}\dot{\lambda}_3}{3}(1 + 2\lambda_3^{-3}) = \frac{\sqrt{2}}{3}\frac{d}{dt}(\lambda_3 - \lambda_3^{-2}) \quad (6)$$

The corresponding equation for the planar extension case is

$$\dot{e}'_{13} = \frac{\sqrt{2}\dot{\lambda}_3}{3\sqrt{a^2 - a + 1}}\left(1 - \frac{a}{2} + \frac{1 + a}{2}\lambda_3^{-2}\right) \quad (7)$$

The two sets of equations (2)–(4) and (5)–(7) provide alternative definitions for the experimentally applied strain rate history $\dot{\lambda}_3$ required to give any constant shear rate $\dot{e}'_{13}$. In either case accelerating testing speeds are required, but the increases in the applied rate during loading are different. The effect of the choice of strain rate measure can be assessed by examining the rate dependence of the stress. A fair estimate can be made from the results at 90°C, where at moderate strain rates a doubling of the rate gives a rise in stress of around 10% (see *Figures 3–5* later). Depending on which set of equations we choose, the rate applied during an experiment will increase by different amounts, but this is never more than a factor of 2; in the equibiaxial and planar experiments, the highest factors are respectively 1.2

and 1.5, and in the uniaxial case the factor approaches 2 at maximum stretch. We can therefore regard the 10% change in stress as an upper limit for the effect of the choice of strain rate measure, and conclude that very similar results would be obtained via the use of either equations (2)–(4) or (5)–(7).

In the uniaxial and equibiaxial cases, the required accelerating rates can be easily programmed into the motor control computers since the extension ratio λ_3 can be calculated from equation (5) or (6) as the experiment proceeds. The planar extension case is more problematic, as ideally the principal stress ratio a should be used to obtain the shear rate and so feedback control would be required. However, there is only a small error produced by the assumption that a is constant. In the experiments we observed that initially $a \approx 1/2$, and at maximum extension $a \approx 1/4$. We assume that $a = 1/3$; this gives rise to an error in the shear rate of around 2% at low and high extensions.

RESULTS AND DISCUSSION

Overall pattern of behaviour

For all types of test there is a qualitative difference in behaviour at the two temperatures of 84 and 90°C. At the lower temperature, within the glass transition range, there is a yielding-type behaviour which manifests itself as an initially high slope in the stress–strain curve followed by a rapid change to a lower slope; this effect is visible in *Figure 2* and is observed at all but the slowest speeds. The effect is absent at 90°C. The general form of the rate dependence is the same at both temperatures, and can be seen in *Figures 3*, *4* and *5* for uniaxial, planar and equibiaxial stretching, respectively.

To deal with the dependence of stress on both strain and strain rate we have adopted the following procedure. It will be assumed that for all testing modes the octahedral shear stress is uniquely determined by the octahedral shear strain and the octahedral shear strain rate. This generalizes for the multiaxial case to the concept of a true stress–strain–strain rate relationship in uniaxial tension, which has proved very useful in the analysis of the mechanics of solid phase polymer processing[7]. Accordingly, in *Figures 3–5* stress in the form of octahedral shear stress is plotted at the same value

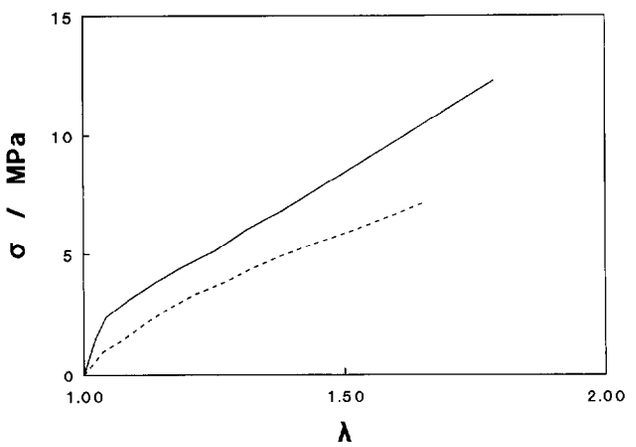

Figure 2 Stress–strain curves for equibiaxial stretching at a constant shear rate of $2 \times 10^{-2}\,s^{-1}$. Note that the initially steep slope in the 84°C plot (——) and its absence at 90°C (– –)

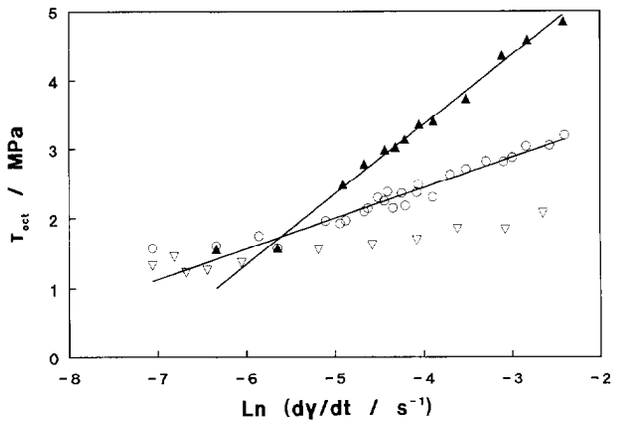

Figure 3 Octahedral shear stress taken at a constant octahedral shear strain and plotted against octahedral shear strain rate for uniaxial stretching: (▲) 84°C; (○) 90°C; (▽) 100°C

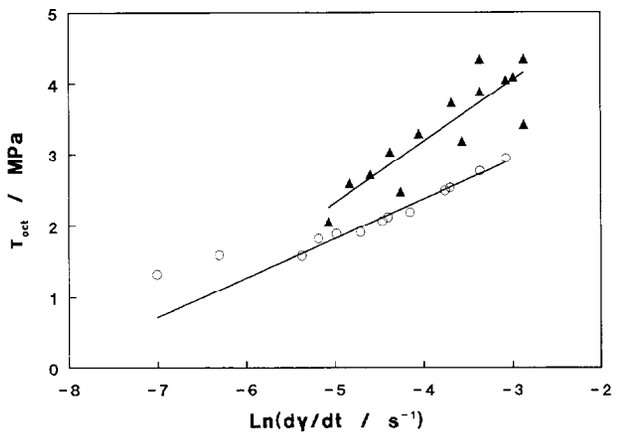

Figure 4 Octahedral shear stress taken at a constant octahedral shear strain (the same value as in *Figure 3*) and plotted against octahedral shear strain rate for planar stretching: (▲) 84°C; (○) 90°C

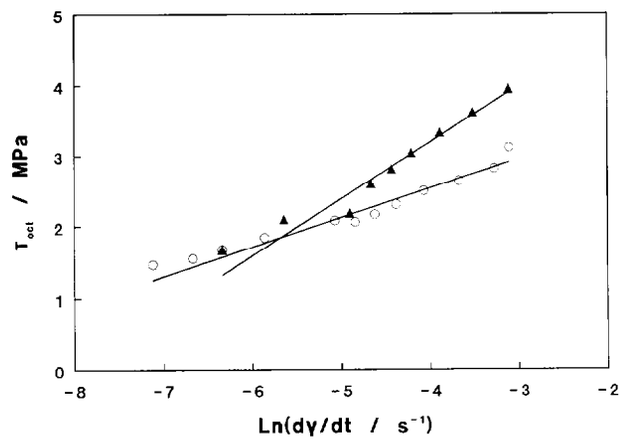

Figure 5 Octahedral shear stress taken at a constant octahedral shear strain (the same value as in *Figure 3*) and plotted against octahedral shear strain rate for equibiaxial stretching: (▲) 84°C (○) 90°C

of octahedral shear strain for a range of shear strain rates. For simplicity we write the octahedral shear strain rate as $\dot{\gamma} = \dot{e}'_{13}$. Then the octahedral shear strains corresponding to the rates given in equations (5)–(7) are for uniaxial stretching

$$\gamma = \frac{\sqrt{2}}{3}(\lambda_3 - \lambda_3^{-1/2}) \tag{8}$$

for equibiaxial stretching

$$\gamma = \frac{\sqrt{2}}{3}(\lambda_3 - \lambda_3^{-2}) \tag{9}$$

and for planar extension

$$\gamma = \frac{\sqrt{2}}{3\sqrt{a^2-a+1}}\left[\left(1-\frac{a}{2}\right)(\lambda_3 - 1) - \frac{1+a}{2}(\lambda_3^{-1} - 1)\right] \tag{10}$$

The same value of γ is used corresponding to λ_3 values of 1.665 in uniaxial extension (*Figure 3*), 1.400 in equibiaxial extension (*Figure 4*) and 1.631 in planar extension (*Figure 5* with $a = 1/3$). All three figures show that there is a linear relation between the stress and $\ln \dot{\gamma}$ for rates in the range $\ln[\dot{\gamma}\ (s^{-1})] > -6$, with the stress apparently independent of strain rate at rates lower than this. In *Figure 3* there are additional points from experiments at 100°C which confirm this general picture. For a given temperature, the slopes and intercepts do not differ significantly for the three stretching modes.

There is thus a threshold strain rate above which the time dependent effects are observed. Below the threshold rate, stress–strain curves at 84 and 90°C are virtually identical. We can use ideas similar to those of Bauwens *et al.*[1] and envisage that below the threshold strain rate, there is sufficient time available for molecular segments to move into pre-existing regions of free volume, whereas above it energy is required to create new voids.

The conventional approach is that the total stress is the sum of network and viscosity components[3,4]. We will show that this model does not fit the present data at 90°C. It would require that the stress below the threshold strain rate be equated with the network stress, and the stress at higher rates be the sum of the network stress plus a viscous component of the form $\sigma = A + B\ln(\dot{\gamma}/\dot{\gamma}_0)$, where $\dot{\gamma}_0$ is the threshold strain rate. This expression, suggested by the form of *Figures 3–5*, is equivalent to Eyring's model with the hyperbolic sine function replaced by an exponential or Argon's model[8] with an exponent of 1 rather than 5/6. A property of such a model, which can be envisaged as a network with an Eyring-like dashpot in parallel, is that after an initial transient period, the stress due to the viscous component becomes constant. Therefore, if we compare the stress in two experiments, one below the threshold strain rate and one above, then the stress–strain curves should run parallel after the initial transient period; the difference between the stresses becomes the constant viscous component. In *Figure 6* we do exactly this. Two equibiaxial experimental curves taken at 90°C are shown, one at a rate corresponding to $\ln[\dot{\gamma}\ (s^{-1})] = -6.4$ and the other at $\ln[\dot{\gamma}\ (s^{-1})] = -3.7$. They do not run parallel. This is not the result of a prolonged transient period, since any values of the constants A and B which approximate reasonably to those suggested by the behaviour seen in *Figures 3–5* give a transient period well within the experimental time span. We are therefore bound to conclude that the simple model of time independent network plus viscous stress fails.

Results at 90°C: the model of Ball et al.

The recognition that the strain rate dependence of the stress could not be attributed to a viscosity component in parallel with the deformation of a simple rubberlike network has led us to examine a model in which the strain rate dependence is an integral part of the behaviour of the network; we introduce the time dependence into the network directly and assume that there is no separate viscosity term. The general characteristics of the behaviour we observe, in which strain hardening is not a significant feature, together with the desire to use a model which is physically based rather than purely phenomenological, have led us to consider as a basis the model of Ball *et al.*[9]. Their network is defined by a strain energy function given by

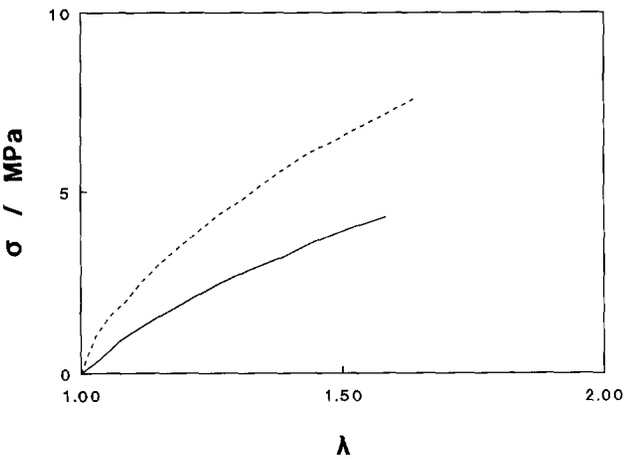

Figure 6 Comparison of stretching curves at 90°C for two constant shear rates: (——) $\dot{\gamma} = 6.2 \times 10^{-3}\ s^{-1}$; (– –) $\dot{\gamma} = 3.8 \times 10^{-2}\ s^{-1}$. The rate dependence occurs in the absence of any initial steep slope

$$\frac{F}{kT} = \frac{1}{2}N_c\Sigma\lambda_i^2 + \frac{1}{2}N_s\Sigma\left[\frac{(1+\eta)\lambda_i^2}{1+\eta\lambda_i^2} + \ln(1+\eta\lambda_i^2)\right] \tag{11}$$

where F is the energy, N_c and N_s are respectively the number of crosslinks and the number of sliplinks, and η is a parameter governing the slipperiness of the sliplinks. Expressions for the stress in any stretching mode are given by

$$\sigma_{ii} = \lambda_i \frac{\partial F}{\partial \lambda_i} + p \tag{12}$$

where p is a hydrostatic pressure. Solving for p in each case gives a set of expressions for the stress in the three stretching modes.

The above model has been applied to the 90°C results. Optimum values of the three parameters can be obtained for individual stress–strain curves by least-squares fitting. The planar extension experiment is the most critical for fitting the model; of the three types of experiment, this corresponds to the most general stress state, with three different principal stresses, and both the non-zero stresses are fitted. In the other two stretching modes there is only one distinct stress and satisfactory fits can be obtained using a wide range of parameter values, with the converse effect being that free fitting of the parameters to the stress–strain curves gives noisy results. When this procedure is applied to both the axial and lateral stresses in constant width tests, it is found that consistently $N_c = 0$ regardless of the strain rate. This makes sense physically for a non-crystalline polymer above its glass transition. Overall, for all three types of test, $N_c = 0$ together with a constant value for η of 0.08 gives a good representation of the data over the whole range of strain rates. According

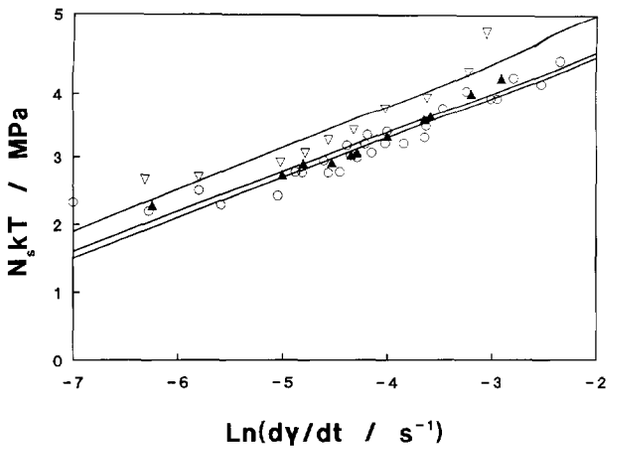

Figure 7 Sliplink number N_s (equation (11) with $N_c=0$ and $\eta=0.08$) for three stretching modes: (○) uniaxial; (▲) planar; (▽) equibiaxial. Each point is obtained by fitting to an experimental stress–strain curve

to the model, the stress is now proportional to N_s, and since we already know (*Figures 3–5*) that the stress is a linear function of the logarithm of the strain rate, it is inevitable that the relation

$$N_s kT = A + B\ln(\dot{\gamma}/\dot{\gamma}_0) \tag{13}$$

should apply for $\dot{\gamma} \geq \dot{\gamma}_0$. When we fit the model to the individual stress–strain curves under the constraints $N_c=0$ and $\eta=0.08$, the resulting values of N_s do indeed show this dependence (see *Figure 7*). The slopes are very similar for all three stretching modes, and the average line forms a good fit to all the data; with $\ln[\dot{\gamma}_0(s^{-1})]=-6$, this line is defined by parameters in equation (13) having the values $A=2.27$ MPa and $B=0.60$ MPa. We can now go back and use this linear relation for N_s and the values $N_c=0$ and $\eta=0.08$ to predict the stress–strain curves in the strain rate interval defined by $-6<\ln[\dot{\gamma}(s^{-1})]<-2$. At lower speeds, a constant value of N_s is used in place of equation (13). Some of the predictions are shown in *Figure 8*. The predictions of stress are extremely good for all three stretching modes over the whole range of strain rates (five decades). The alternative of keeping N_s constant and allowing η to vary with the strain rate did not produce successful predictions.

It has been shown that the deformation behaviour of PVC at 90°C can be represented by a model in which the stress–strain behaviour and the strain rate dependence are separable. The time dependent behaviour has been directly incorporated within the network model, suggesting that it is associated with the dynamics of the deformation behaviour at a molecular level, for example in the motions of the chains under large deformations.

Results at 84°C: retention of the sliplink network of Ball et al. *with the introduction of elastic and viscous components*

It is clear from the coincidence of the data for deformation at low strain rates that deformation at the lower temperature of 84°C must involve the stretching of the same network as at 90°C. At higher strain rates we observe the qualitative difference in the behaviour at 84°C, with the presence of the initial steep response in the stress–strain curve. The question arises as to whether we can explain the observed shape of the stress–strain curves at this lower temperature using only the form of time dependence as in the dynamic network model discussed above. The results clearly suggest the existence of an initial elastic response. As a first step, we split the total deformation by multiplicative decomposition, i.e.

$$\lambda_i = \lambda_i^e \lambda_i^n \qquad (i=1, 2 \text{ and } 3) \tag{14}$$

into the elastic stretch and network stretch λ_i^e and λ_i^n, respectively. This corresponds to the rate equation

$$\frac{\dot{\lambda}_i}{\lambda_i} = \frac{\dot{\lambda}_i^e}{\lambda_i^e} + \frac{\dot{\lambda}_i^n}{\lambda_i^n} \qquad (i=1, 2 \text{ and } 3) \tag{15}$$

We then assume an isotropic elastic response in the form

$$\begin{aligned} \ln\lambda_1^e &= s_d\sigma_{11} + s_c\sigma_{33} \\ \ln\lambda_2^e &= s_c(\sigma_{11}+\sigma_{33}) \\ \ln\lambda_3^e &= s_c\sigma_{11} + s_d\sigma_{33} \end{aligned} \tag{16}$$

where s_d and s_c are respectively the normal compliance and the lateral compliance. The network response σ_{ii}^n is obtained from equation (12) by noting that $\sigma_{22}=0$ and eliminating p using $\sigma_{ii}^n=\sigma_{ii}^n-\sigma_{22}^n$ ($i=1$ and 3)

This gives stresses in the form

$$\sigma_{ii}^n = \begin{cases} [A+B\ln(\dot{\gamma}/\dot{\gamma}_0)]f(\lambda_i^n, \lambda_2^n) & (\dot{\gamma}\geq\dot{\gamma}_0) \\ Af(\lambda_i^n, \lambda_2^n) & (\dot{\gamma}\leq\dot{\gamma}_0) \end{cases} \qquad (i=1 \text{ and } 3) \tag{17}$$

Here the function f incorporates derivatives of the strain energy function F. For the simplest model which includes both a network and an elastic response, we assume $\sigma_{ii}^n=\sigma_{ii}$. Then equations (15)–(17) represent a mechanical model equivalent to an elastic spring in series with the dynamic network established for the 90°C experiments. The system of equations is equivalent to a differential equation in stress or extension ratio and we have explored its dynamics using numerical methods. Its behaviour does not correspond to that observed, in that no credible choice of parameters can produce the initial steep response seen in *Figure 2*.

However, the required behaviour can be obtained by introducing an additional Eyring-like viscosity term. Adding such a viscosity in parallel with the network is equivalent to the assumption that

$$\sigma_{ii} = \sigma_{ii}^n + \sigma_{ii}^p \qquad (i=1 \text{ and } 3) \tag{18}$$

where the superscript p denotes the plastic or viscous component of stress. The total stress is still defined by the elastic equations (16). The model can be represented conceptually by the arrangement in *Figure 9*. Note that while the network and plastic components have the same state of deformation as defined by the extension ratios λ_i^n, the octahedral shear strain rates are in general different, since these quantities depend on the state of stress. Specifically, defining principal stress ratios for the network and plastic terms, respectively, by

$$\sigma_{11}^n = a_n\sigma_{33}^n \quad \text{and} \quad \sigma_{11}^p = a_p\sigma_{33}^p \tag{19}$$

enables us to write octahedral shear rates as

$$\dot{\gamma}_n = \frac{\sigma_{33}^n}{9\tau_{oct}^n}[\dot{\lambda}_1^n(2a_n-1) - \dot{\lambda}_2^n(1+a_n) + \dot{\lambda}_3^n(2-a_n)] \tag{20}$$

$$\dot{\gamma}_p = \frac{\sigma_{33}^p}{9\tau_{oct}^p}[\dot{\lambda}_1^n(2a_p-1) - \dot{\lambda}_2^n(1+a_p) + \dot{\lambda}_3^n(2-a_p)] \tag{21}$$

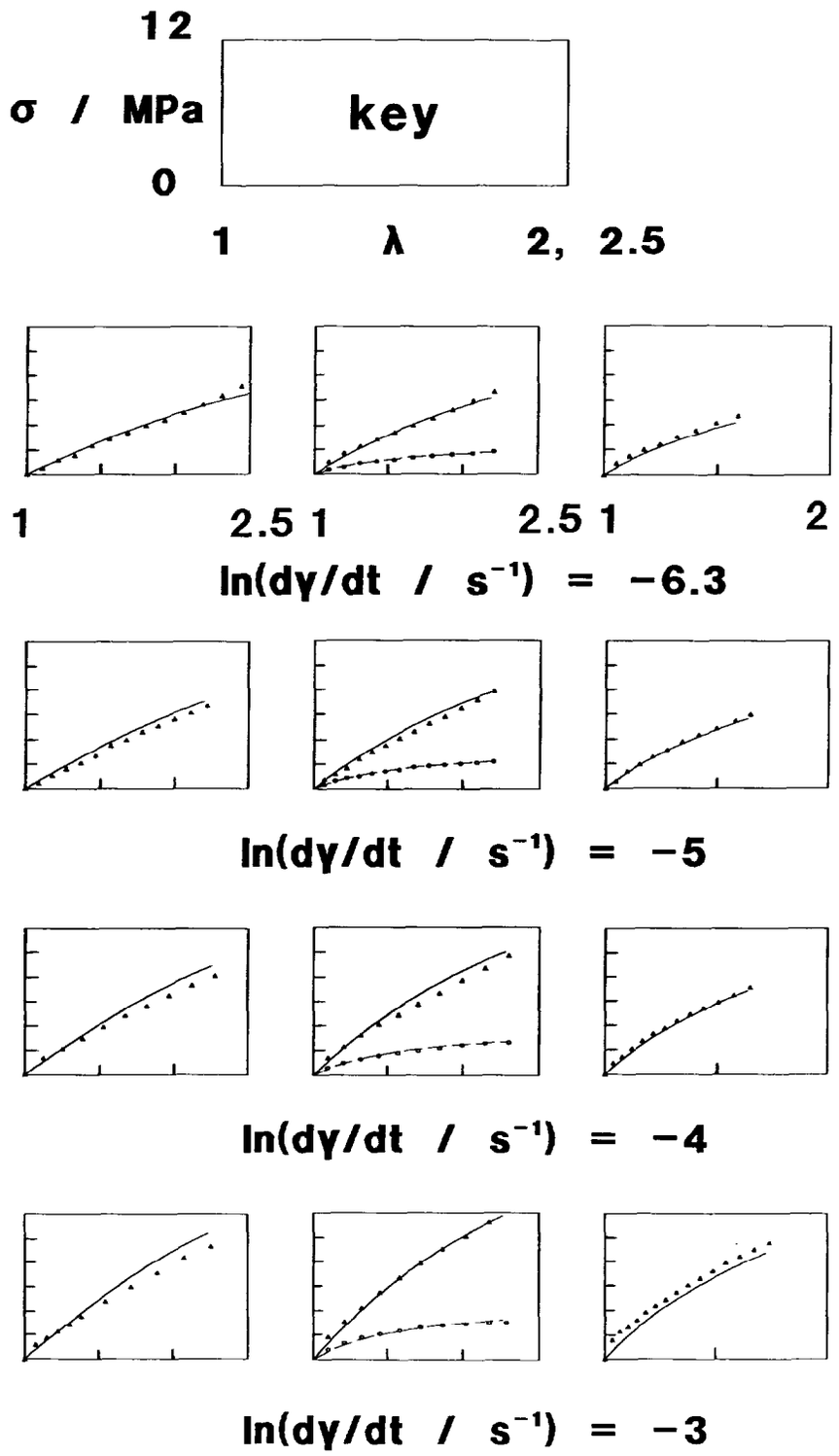

Figure 8 Experimental stresses (points) and predictions (lines) obtained with the model of Ball *et al.* with the sliplink number N_s given by equation (13) for $\ln \dot{\gamma} \geq -6$, otherwise constant. Uniaxial, planar and equibiaxial curves are presented from left to right. Stresses are σ_3 (▲, ——) and, for planar extension, σ_1 (○, – –). Strain rate increases from the top of the figure

using the same analysis as for the derivation of equation (1). The octahedral shear stresses are now

$$\tau^{n}_{oct} = \tfrac{1}{3}\sqrt{2[(\sigma^{n}_{11})^2 + (\sigma^{n}_{33})^2 - \sigma^{n}_{11}\sigma^{n}_{33}]}$$
$$\tau^{p}_{oct} = \tfrac{1}{3}\sqrt{2[(\sigma^{p}_{11})^2 + (\sigma^{p}_{33})^2 - \sigma^{p}_{11}\sigma^{p}_{33}]} \qquad (22)$$

The network stress is obtained by rewriting equation (17)

$$\sigma^{n}_{ii} = \begin{cases} [A + B\ln(\dot{\gamma}_n/\dot{\gamma}_0)]f(\lambda^{n}_1, \lambda^{n}_2) & (\dot{\gamma} \geq \dot{\gamma}_0) \\ Af(\lambda^{n}_1, \lambda^{n}_2) & (\dot{\gamma} \leq \dot{\gamma}_0) \end{cases} \quad (i = 1 \text{ and } 3) \qquad (23)$$

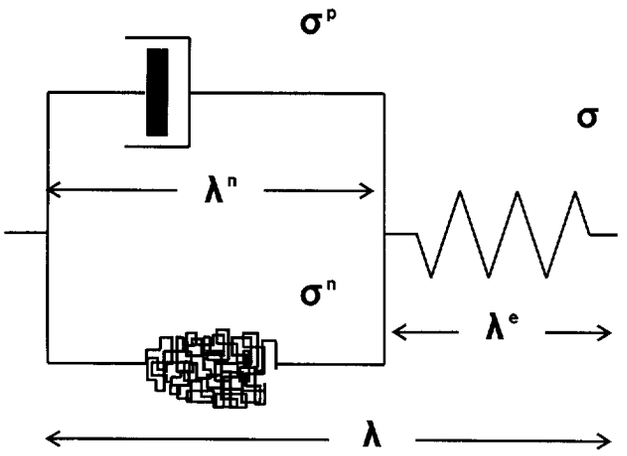

Figure 9 Representation of the model for use at 84°C. A viscous dashpot (equation (24)) is in parallel with a time dependent network (equation (23)) and in series with an elastic response (equation (16))

The viscous stress is prescribed in terms of the shear rate and a material constant D

$$\tau^{p}_{oct} = D \ln(\dot{\gamma}_p/\dot{\gamma}_0) \tag{24}$$

To prescribe fully the plastic deformation requires the addition of a flow rule. We assume that the true principal plastic strain rates are in proportion with the components of the plastic stress deviator, so that (bearing in mind that the network and plastic deformation states are identical)

$$\begin{bmatrix} \dot{\lambda}^n_1/\lambda^n_1 & 0 & 0 \\ 0 & \dot{\lambda}^n_2/\lambda^n_2 & 0 \\ 0 & 0 & \dot{\lambda}^n_3/\lambda^n_3 \end{bmatrix} = \alpha \begin{bmatrix} 2a_p - 1 & 0 & 0 \\ 0 & -(1+a_p) & 0 \\ 0 & 0 & 2-a_p \end{bmatrix} \tag{25}$$

where α is a constant. This enables us to express the rates in the 1 and 2 directions in terms of the rate in the 3 direction

$$\dot{\lambda}^n_1 = \frac{\lambda^n_1 \dot{\lambda}^n_3 (1-2a_p)}{\lambda^n_3 (a_p - 2)}$$

$$\dot{\lambda}^n_2 = \frac{\lambda^n_2 \dot{\lambda}^n_3 (1+a_p)}{\lambda^n_3 (a_p - 2)} \tag{26}$$

The assumption of incompressibility is implicit in these relations, and for the uniaxial case ($a_p = 0$) and the equibiaxial case ($a_p = 1$) they return the appropriate result; thus, for these special cases any flow rule consistent with incompressibility would suffice. The flow rule given here appears to be the simplest possibility which is compatible with this requirement.

The above equations can be combined to form a differential equation which is solved numerically to give the total stress as a function of extension. In the planar extension case, iterative procedures are used to give convergent values of the stresses and a_n and a_p; equations (18), (20)–(24) and (26) are combined to give a relation between the total stress and the network extension rate, and the total stress is also related to the known total extension and the network extension via equations (14) and (16). In the uniaxial and equibiaxial cases the quantities a_n and a_p are known and the procedure is relatively trivial.

Material data required are η (equation (11)), $\dot{\gamma}_0$ (equations (13) and 23)), s_d and s_c (equations (16)), A and B (equations (13) and (23)), and D (equation (24)). We set $\eta = 0$ to give the best fit to the data. *Figures 3–5* do not reveal any change in the threshold strain rate $\dot{\gamma}_0$ between 84 and 90°C, and in equations (13) and (23) we have already assumed that the same quantity is appropriate for both network and viscous stress. We use the value suggested by the behaviour of N_s as seen in *Figure 7*, i.e. $\ln[\dot{\gamma}_0(s^{-1})] = -6$. The initial slopes of the stress–strain curves are used to fix the values of s_d and s_c at respectively 0.02 and $-0.008\ \mathrm{MPa}^{-1}$. The quantities A and B are fitted by trial and error to the values 2.31 and 0.8 MPa, respectively, similar to the values at 90°C. By the same process we arrive at $D = 0.6$ MPa.

Typical results are shown in *Figure 10*, where the numerical predictions are compared with the observed stress–strain curves for a planar extension experiment. The initial transient parts of the curves are modelled well and overall the fit is good. At higher draw ratios, there is some deviation when the experimental curve begins to slope upwards: this appears to be the onset of strain hardening. This is not modelled by the theory since the network has no strain-hardening properties. The sliplink network is being used with the parameter $\eta = 0$, which corresponds to the extreme case of a classical phantom network. It would probably be more appropriate to use a theory with the potential for strain hardening rather than push the present model to its limit – an obvious choice would be the theory of Edwards and Vilgis[10], which generalizes the model of Ball *et al.* to include finite chain extensibility. In *Figure 11*, we show results for a range of strain rates and all three stretching modes. Apart from the small deviations due to strain hardening, the predictions are very good. The greatest strain rate shown corresponds to $\ln[\dot{\gamma}(s^{-1})] = -3$; this is the fastest rate possible without early tearing of the equibiaxial specimen. Good fits are still obtained with the uniaxial specimens at the highest rate obtainable, which corresponds to $\ln[\dot{\gamma}(s^{-1})] = -2.5$.

According to the numerical results, the greatest value of λ^e_3 is about 1.3, occurring at the maximum extension. For the planar extension cases, we find that the greatest difference between the network and viscous strain rates

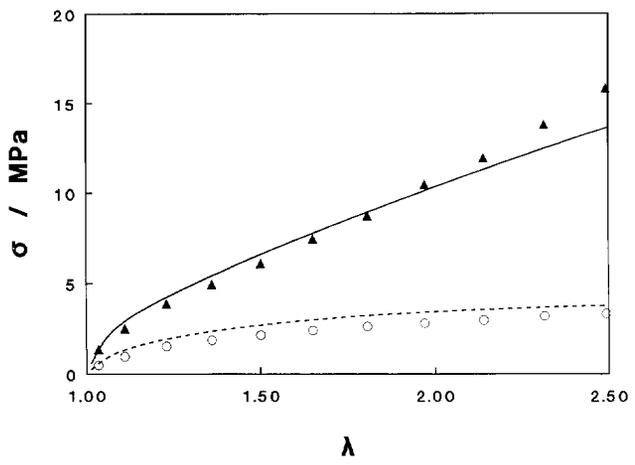

Figure 10 Planar extension at 84°C at a rate $\dot{\gamma} = 1.4 \times 10^{-2}\ s^{-1}$. Observed stresses are given by points (σ_3, ▲; σ_1, ○) and predictions by lines (σ_3, ——; σ_1, – –). The increasing slope of the experimental curves at higher draw ratios is thought to be associated with strain hardening of the network

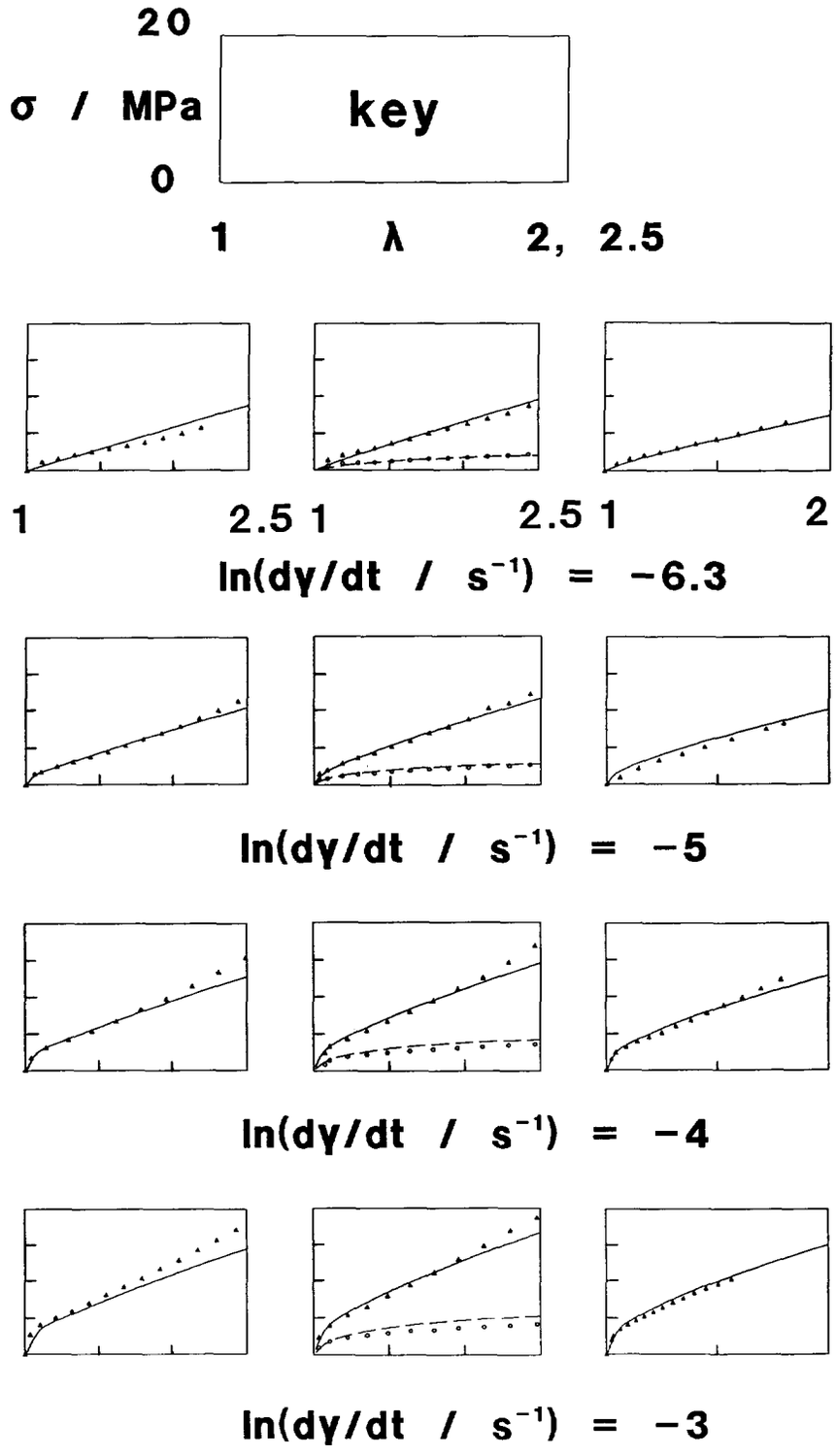

Figure 11 Experimental stresses (points) and predictions (lines) obtained with the model of *Figure 9*. Uniaxial, planar and equibiaxial curves are presented from left to right. Stresses are σ_3 (▲, ——) and, for planar extension, σ_1 (○, – –). Strain rate increases from the top of the figure

corresponds to $\dot{\gamma}_n \approx 1.06\dot{\gamma}_p$. As noted above, the network and viscous states of deformation as defined by the stretch ratios are the same, and these two rates differ only as a result of the octahedral planes defined by the plastic and network stress states being different. We would therefore not expect the network and viscous strain rates to differ by much. Our result confirms this, and shows that the consequences of their being allowed to be independent have not been great.

The parameter D can be interpreted in terms of an activation volume. The exponential approximation to the Eyring equation can be written as

$$\dot{\gamma}_p = \dot{\gamma}'_0 \exp\left(\frac{\tau_{oct} v - \Delta H}{kT}\right)$$

where $\dot{\gamma}'_0$ differs from $\dot{\gamma}_0$ by a constant, v is the activation volume, ΔH the activation enthalpy, k the Boltzmann

constant and T the absolute temperature. Comparing this with equation (24) leads to the relation

$$v = \frac{kT}{D}$$

from which the value $D = 0.6$ MPa results in an activation volume of 8.2 nm^3. This compares favourably with the value of 8.6 nm^3 quoted for PVC by Haward and Thackray[11].

Overview

The stress is dependent on the strain rate, but different forms of dependence are observed at the two temperatures. The model of a viscosity mechanism acting in parallel with a rate independent network, useful for glassy polymers below the glass transition, is found to be unsustainable for this material at 90°C. The rate dependence at this temperature is modelled well by embedding it within the network model by means of a sliplink number N_s which is a function of strain rate. However, at the lower temperature of 84°C the use of a viscosity term in parallel with the network is essential, while we still retain the rate dependence incorporated into the network. Here, we also include an elastic term which is absent in our representation of the 90°C behaviour. This is not because we believe there to be no elastic process at 90°C, but rather that its effects, which are manifest mainly in the initial transient behaviour at 84°C, are not observable in the absence of a viscous process in our monotonic loading experiments.

The values for the sliplink number N_s which we have found and used above correspond to about one sliplink per 30 repeat units. The dependence of N_s on rate suggests that the parameter may in part correspond to short-lived interactions. In the context of stretching of polyethylene, Brereton and Klein[12] have noted a clear strain rate dependence for N_s.

The Eyring-like viscous behaviour seen at 84°C is well established for the yield behaviour of polymers below the glass transition. Plastic shearing is assumed to take place as a result of molecules or molecular segments acquiring activation energy to surmount potential barriers presented by adjacent material, with the net effect resembling that of individual molecular chains moving through a viscous fluid. We can envisage that at 90°C, the increased free volume associated with the glass transition eliminates this effect, so that molecular chains are able to move more freely, like the elements of a network. There remains the question of why the number of sliplinks should show the observed dependence on strain rate. We note that N_s depends on the same rate parameter, $\ln(\dot{\gamma}/\dot{\gamma}_0)$, as does the viscous stress at 84°C, and this suggests a mechanism involving similar molecular motions. We propose that while there is sufficient free volume at 90°C to enable the flexing of molecular chains, the sliplinks, which consist of larger molecular entanglements, perceive the surrounding medium as a viscous fluid in much the same way as the molecular chains at the lower temperature, and their motion is resisted. In sliplink theories, the sliplinks are considered as fixed in positions determined by affine transformations, but some motion away from these positions could be induced by forces from the chains which the sliplinks constrain, which would in the process be relaxed. For a sliplink to remain effective, the force on it should be less than that required to cause it to move through the material. The required force is associated with a viscous process and therefore proportional to $\ln(\dot{\gamma}/\dot{\gamma}_0)$. For a total number of entanglements N_e, the number of effective sliplinks N_s can be estimated as

$$N_s = \sum_{i=1}^{N_e} j | j = 1 \text{ when } f_i < A_i \ln(\dot{\gamma}/\dot{\gamma}_0), \text{ otherwise } 0$$

where f_i is the force exerted by the chains on each site and A_i is a parameter which in general can be different for each i. Assuming a rectangular distribution for the forces f_i, and all the A_i to be the same, we obtain an expression of the form

$$N_s = B \ln(\dot{\gamma}/\dot{\gamma}_0)$$

up to the maximum value N_e. Assuming instead that the A_i are such that there are a number of sliplinks which are fixed in terms of affine deformation results in

$$N_s = A + B \ln(\dot{\gamma}/\dot{\gamma}_0)$$

i.e. the observed relation. While the ideas are crude at this stage, they fit the observations in a plausible way. The observed strain rate dependence at 90°C is linked with the motion of the sliplinks, and it is therefore of interest to derive the activation volume for this process. The rate dependences suggest a value of 10.6 nm^3; this is slightly higher than the 8.6 nm^3 corresponding to the viscous process at 84°C, which on this interpretation is associated with chain motions.

CONCLUSIONS

The form of the rate dependence of the results at 90°C forces us to include rate dependence in the network model. The important feature of the form of this dependence is the separability of the stress response into a product of a function of strain and a function of strain rate. Use of this separability has precedents in the field of polymer deformation[13,14]. At the lower temperature, the inclusion of time dependence within the network is the main conceptual departure from the work of Boyce *et al.*[4]; otherwise, the formulation is similar.

The material shows contrasting behaviour at 84 and 90°C. The stresses are dependent on strain rate at both temperatures. The concept of a viscous mechanism operating in parallel with a network is found to be necessary at the lower temperature, where there is an initial elastic response in the stress–strain curves; however, the same concept is of no use in modelling the rate dependence at 90°C. Here, time dependence is introduced successfully into the network model of Ball *et al.*[9] by making the sliplink number a function of rate. Then, the behaviour at 84°C is modelled by the same kind of network acting in parallel with an Eyring-like viscosity and in series with an isotropic linear elastic term.

It is natural to associate the difference in behaviour with the glass transition, which occurs in the range 77–85°C. At 84°C, the viscous term gives a stress which depends only on the strain rate and so is observed from the onset of straining. At the higher temperature, this term is absent and the rate dependence develops with the deformation, with the total stress separable into a product of functions of strain rate and strain. The difference in

behaviour may be associated with the increase in free volume above the glass transition.

The models used at both temperatures give excellent representations for all three stretching modes over a wide range of strain rates. The planar extension test provides a much more discriminating test of theory than do the uniaxial or biaxial tests in that a satisfactory fit to theory is generally possible only over a narrower range of parameters.

REFERENCES

1 Bauwens, J. C., Bauwens-Crowet, C. and Homès, G. *J. Polym. Sci. A-2* 1969, **7**, 1745
2 Padibjo, S. R. and Ward, I. M. *Polymer* 1983, **24**, 1103
3 Ward, I. M. *Polym. Eng. Sci.* 1984, **24**, 724
4 Boyce, M. C., Parks, D. M. and Argon, A. S. *Int. J. Plast.* 1989, **5**, 593
5 Sweeney, J. and Ward, I. M. *Trans. Inst. Chem. Eng. A* 1993, **71**, 232
6 Karacan, I., Bower, D. I. and Ward, I. M. *Polymer* 1994, **35**, 3411
7 Coates, P. D. and Ward, I. M. *J. Mater. Sci.* 1980, **15**, 2897
8 Argon, A. S. *Philos. Mag.* 1973, **28**, 839
9 Ball, R. C., Doi, M., Edwards, S. F. and Warner, M. *Polymer* 1981, **22**, 1010
10 Edwards, S. F. and Vilgis, Th. *Polymer* 1986, **27**, 483
11 Haward, R. N. and Thackray, G. *Proc. R. Soc. London, Ser. A* 1968, **302**, 453
12 Brereton, M. G. and Klein, P. G. *Polymer* 1988, **29**, 970
13 Marquez-Lucero, A., G'sell, C. and Neale, K. W. *Polymer* 1989, **30**, 636
14 Marquez-Lucero, A. and G'sell, C. *Polymer* 1993, **34**, 2740